In situ x-ray-absorption spectroscopy study of hydrogen absorption by nickel-magnesium thin films

B. Farangis,[1] P. Nachimuthu,[2,3] T. J. Richardson,[1,*] J. L. Slack,[1] R. C. C. Perera,[2] E. M. Gullikson,[2] D. W. Lindle,[3] and M. Rubin[1]

[1]*Environmental Energy Technologies Division, Lawrence Berkeley National Laboratory, Berkeley, California 94720*

[2]*Center for X-ray Optics, Materials Sciences Division, Lawrence Berkeley National Laboratory, Berkeley, California 94720*

[3]*Department of Chemistry, University of Nevada, Las Vegas, Nevada 89154*

(Received 16 July 2002; revised manuscript received 22 October 2002; published 25 February 2003)

Structural and electronic properties of co-sputtered Ni-Mg thin films with varying Ni to Mg ratio were studied by *in situ* x-ray absorption spectroscopy in the Ni *L*-edge and Mg *K*-edge regions. Codeposition of the metals led to increased disorder and decreased coordination around Ni and Mg compared to pure metal films. Exposure of the metallic films to hydrogen resulted in formation of hydrides and increased disorder. The presence of hydrogen as a near neighbor around Mg caused a drastic reduction in the intensities of multiple scattering resonances at higher energies. The optical switching behavior and changes in the x-ray spectra varied with Ni to Mg atomic ratio. Pure Mg films with Pd overlayers were converted to MgH_2: The H atoms occupy regular sites as in bulk MgH_2. Although optical switching was slow in the absence of Ni, the amount of H_2 absorption was large. Incorporation of Ni in Mg films led to an increase in the speed of optical switching but decreased maximum transparency. Significant shifts in the Ni L_3 and L_2 peaks are consistent with strong interaction with hydrogen in the mixed films.

DOI: 10.1103/PhysRevB.67.085106 PACS number(s): 61.10.Ht, 78.20.−e, 78.66.−w, 82.30.−b

I. INTRODUCTION

Switchable mirrors exhibiting variable optical, mechanical, and electrical properties due to uptake and removal of hydrogen were discovered by Huiberts *et al.*[1] They have significant potential for applications in light and heat regulation, display devices, and optical communication systems. The first generation of switchable mirrors was based on rare earth metals that undergo a reversible metal-insulator transition when thin films coated with palladium are exposed to H_2.[2] van der Sluis, Ouwerkerk, and Duine[3] reported that incorporation of magnesium increased the transparency of lanthanide hydride films. The larger optical band gap (3.4 eV) for $Gd_{0.5}Mg_{0.5}H_{2.5}$ makes this switchable mirror colorless in contrast to reddish GdH_3. Recently Richardson *et al.*[4,5] reported switchable mirror effects in thin films of Mg and 3*d* transition metals (Ni, Mn, Fe, and Co). These are potentially more cost effective since they do not require the expensive and reactive rare-earth metals.

A recent report[6] on the hydrogenation of 200-nm-thick Mg films with Pd over-layers by H_2 gas at 0.1 MPa and 100 °C showed that magnesium hydride is formed, with H_2 loading ranging from 2.9 to 6.6 wt %. After 24 h transparent magnesium hydride was obtained.[7] The temperature required for dehydrogenation decreased with decreasing degree of crystallization. Heating the hydride film led to the formation of nanostructured magnesium. H_2 absorption leads to lattice expansion and structural rearrangements, which modify the electronic properties of the films.

Near-edge x-ray absorption fine structure (NEXAFS) and extended x-ray absorption fine structure (EXAFS) are powerful tools for understanding the electronic and structural properties of thin films.[8–10] These techniques are element-specific and capable of probing the short- to medium-range structure around an absorbing atom. Among the experimental techniques employed in determining the valence states of atoms in solids, NEXAFS plays a crucial role due to its simplicity and universal applicability. EXAFS is sensitive to the local structure around an atom and is especially useful in studying amorphous materials.

X-ray absorption spectroscopy (XAS) and x-ray magnetic circular dichroism (XMCD) are used to study the electronic and magnetic properties of 3*d* elements. Theoretical and experimental studies have shown that the band structure of bulk Ni is different from that of Ni thin films grown on Cu and Co.[11–14] This results in different electronic and magnetic properties. The line shapes of XAS and XMCD spectra can change dramatically for varying film thickness due to electron transfer and hybridization at the interface or due to 3*d* electron correlation effects.[15] Srivastava *et al.*[16] have shown that the thickness-dependent density of 3*d* holes for Ni thin films grown on Cu(001) gives rise to a modified XAS line shape. Therefore a detailed analysis of Ni $L_{2,3}$ edges (which is a direct measure of unoccupied *d* states) and Mg *K* edge are a useful approach to study the electronic structure of our samples in the metallic and hydride state.

Here we report an investigation of the structural and electronic properties of Ni-Mg thin films with varying Ni to Mg atomic ratio using *in situ* x-ray absorption spectroscopy. The mirrorlike metallic Ni-Mg thin films become optically transparent due to H_2 absorption. We followed the hydrogenation processes by recording x-ray absorption spectra at both the Mg *K* and Ni *L* edges.

II. EXPERIMENTAL PROCEDURE

A. Sample preparation

Ni-Mg films for the present study were prepared by dc magnetron cosputtering from 50-mm Ni and Mg (99.98%)

targets inclined 22.5° from normal onto silicon nitride membrane substrates (Silson Ltd., Northampton, UK), which were mounted sequentially on a glass plate to obtain different Ni to Mg atomic ratios. The base pressure was 1.4×10^{-7} Torr, process pressure 2 mTorr, Ni power 24 W, Mg power 47 W, and target-to-substrate distance 7.5 cm. Deposition rates ranged from 0.33 to 0.55 nm/s, depending on location of the substrate. Palladium was deposited over all Ni-Mg films to protect them from air oxidation and to promote absorption of hydrogen. The Pd overlayer was applied at 10 mTorr, Pd power 12.4 W, with deposition rate of 0.16 nm/s. Film thicknesses and compositions were measured by stylus profilometry and Rutherford backscattering (RBS). Mg_2Ni (containing 20% excess Mg) was purchased from Ergenics, Inc., (Ringwood, NJ) and MgH_2 (nominal purity 90%, remainder Mg) from Aldrich Chemical Co. (Milwaukee, WI). Powder x-ray diffraction patterns (XRD) for these compounds confirmed their bulk compositions and purity. Only broad x-ray diffraction peaks due to Pd were observed in all sputtered films.

B. X-ray absorption measurements

The x-ray absorption spectra were measured at beamlines 6.3.1 and 6.3.2 at the Advanced Light Source, Lawrence Berkeley National Laboratory.[17] During the measurements, the synchrotron was typically operated at 1.9 GeV between 200 and 400 mA. The spectra were recorded at the Mg *K* and Ni *L* absorption edges in the bulk-sensitive transmission detection mode, in an atmosphere of He using a 4.6×4.6-mm^2 photodiode detector (Hamamatsu, G1127-02). Hydrogenation of the films was achieved by purging with 4% H_2 in He. The spectra for reference materials Mg_2Ni and MgH_2 were measured by total fluorescence yield (TFY) using a $28 \times 28\ mm^2$ windowless detector (Hamamatsu, S3584-06). The resolution at the Mg *K* and Ni *L* edges was better than 1.5 and 1.0 eV, respectively. The photon energy was calibrated to the first inflection point of the Ni L_3 edge at 852.7 eV and Mg *K* edge at 1303.0 eV.[18] After calibration, the spectra were normalized to the absorption edge jumps.[8] All measurements were performed at room temperature.

III. RESULTS AND DISCUSSION

Previous work[3] on Ni-Mg thin films showed that the Ni to Mg atomic ratio and the film thickness are factors in determining the speed at which switching takes place between the metallic state and the transparent hydride state. The freshly sputtered films were amorphous by XRD, showing only weak reflections due to Pd. Codeposition from offset sources yielded films with position-dependent Ni-Mg atomic ratio and thickness. They absorbed hydrogen rapidly and reached maximum transparency within a few minutes. When samples were annealed at 125 °C in dry nitrogen, XRD reflections due to Mg_2Ni, Mg, and Mg_6Pd developed. The annealed films did not take up H_2 readily.

A. Ni $L_{3,2}$-edge NEXAFS

Ni $L_{3,2}$-edge x-ray absorption spectra measured in transmission mode in He and in 4% H_2 (balance He) for a pure Ni film and two Ni-Mg films are shown in Fig. 1. The spectrum of bulk Mg_2Ni powder measured by total fluorescence yield is included for comparison. The transitions denoted as L_3 and L_2, at ~853.5 and ~870.8 eV, are from Ni $2p_{3/2}$ and $2p_{1/2}$ to $3d$ final states, respectively.[15,18,19] Exposure of the pure Ni film to hydrogen had no effect on its spectrum. Hydrogen absorption by the mixed metal films caused the peak positions to shift to higher energy by more than 2 eV (Table I), with a slightly larger shift in the case of the film with higher Mg content. Since it is difficult to prepare bulk Mg_2Ni without an excess of Mg, it may be that not all of the Ni in the stoichiometric film has participated in the hydriding reaction. The intensity of the 6-eV satellites for Ni-Mg films and Mg_2Ni were reduced by a factor of 5 compared to pure Ni film. Recently Dhesi *et al.*[19,20] assigned this satellite to transitions to singlet states of the final $2p^5 3d^9$ configuration. More recently, Nesvizhskii *et al.*,[21] based on one-electron multiple scattering and atomic multiplet calculations, claimed that the effect of the spin-flip transition is negligible and hence the 6-eV satellite is predominantly due to a multiple scattering effect. The reduced intensity for the 6-eV satellite observed for Ni-Mg films in the present study is therefore attributed to a decreased multiple scattering due to the presence of Mg and the amorphous character of the films.

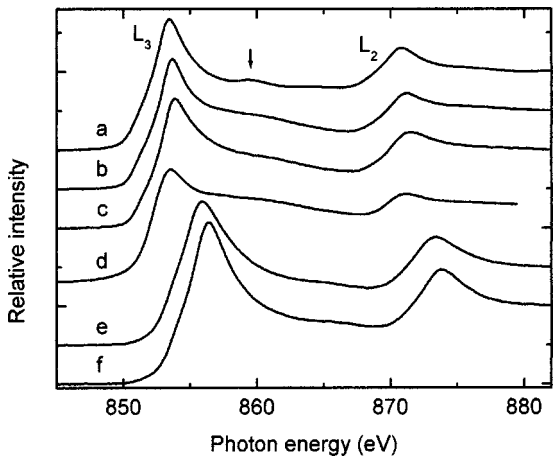

FIG. 1. Ni $L_{3,2}$-edge transmission mode NEXAFS spectra of thin films measured in He: (a) pure Ni (100-nm film with 20-nm Pd), (b) $Ni_{0.33}Mg_{0.67}$ (154-nm film with 11-nm Pd), and (c) $Ni_{0.13}Mg_{0.87}$ (232-nm film with 11-nm Pd); in 4% H_2 in He: (e) $Ni_{0.33}Mg_{0.67}$ and (f) $Ni_{0.13}Mg_{0.87}$. Spectrum (d) Mg_2Ni measured by total fluorescence yield in vacuum. The 6-eV satellite is indicated by arrow. All spectra were normalized to the background. Baselines were shifted for clarity of presentation.

Time-resolved spectra were recorded at both Mg *K* and Ni *L* edges during hydrogen loading of films. Ni $L_{3,2}$ spectra of $Ni_{0.24}Mg_{0.76}H_x$ at different exposure times are presented in Fig. 2. The spectrum denoted as ''end of hydrogenation'' was recorded after exposure to hydrogen for 24 h. Further exposure produced no changes in the spectrum. H_2 absorption led to a shift towards higher energy and an enhancement in intensity. The extent of both effects depended upon exposure time and Ni:Mg ratio. The time required to reach saturation, corresponding to the optical switching from mirror state to maximum transparency, also depended on the film thickness.

TABLE I. Transition energies (E), integrated areas (A), full width at half maximum (FWHM), branching ratios, $\beta_R = A_3/(A_3+A_2)$, total integrated intensities (A_3+A_2), and intensity ratios (A_3/A_2) for Ni $L_{3,2}$-edge XAS of the samples under this study.

	L_3		L_2		FWHM			
Sample	E_3 (eV)	A_3 (a.u.)	E_2 (eV)	A_2 (a.u.)	(eV)	β_R	A_3+A_2 (a.u.)	(A_3/A_2)
100-nm Ni+20-nm Pd[a]	853.5	2.02	870.8	0.66	3.1	0.754	2.68	3.06
154-nm $Ni_{0.33}Mg_{0.67}$+11-nm Pd[a]	853.7	0.88	871.0	0.20	2.0	0.816	1.08	4.40
232-nm $Ni_{0.13}Mg_{0.87}$+11-nm Pd[a]	853.9	1.01	871.1	0.19	2.3	0.840	1.2	5.32
Mg_2Ni powder[b]	853.2	1.70	870.3	0.37	3.2	0.821	2.07	4.60
154-nm $Ni_{0.33}Mg_{0.67}$+11-nm Pd[c]	856.0	2.55	873.4	0.81	3.9	0.758	3.36	3.15
232-nm $Ni_{0.13}Mg_{0.87}$+11-nm Pd[c]	856.5	3.07	873.9	0.99	3.6	0.757	4.06	3.10

[a]XAS measured in transmission mode in He atmosphere.
[b]Total fluorescence yield (TFY) under vacuum.
[c]XAS measured in transmission mode in 4% H_2 in He atmosphere.

Figure 3 shows Ni $L_{3,2}$ spectra for a $Ni_{0.24}Mg_{0.76}$ film as-deposited, fully hydrogenated, and dehydrogenated by exposure to air for 24 h. While the hydriding process is apparently not completely reversible under these conditions, the film has returned very nearly to its original state.

The full width at half maximum (FWHM) and integrated area for each band were obtained by fitting the Ni L-edge spectra with Gaussian functions. To exclude the edge jump, asymmetric double sigmoidal functions were also included in the fits. The results, along with branching ratios $\beta_R = A_3/(A_3+A_2)$, total integrated intensity (A_3+A_2), and intensity ratio (A_3/A_2), are given in Table I. It has been shown that, due to changes in the final-state energies, Ni $L_{3,2}$ transitions shift towards higher energy by about 1 eV for each unit increase in oxidation state.[22–25] Since the integrated intensity (A_3+A_2) is a ground-state property, it is a quantitative and a direct measure of $3d$ shell vacancies (n_h).[16,19,22,24] Further, the initial state $3d$ spin-orbit coupling and the overlap of $2p$ and $3d$ wave functions, the so-called multiplet effects, are said to affect the branching ratio (β_R).[26,27] Another report, however, maintains that multiplet effects dominate all other interactions.[28] Recent reports demonstrate that one can distinguish the nature of spin states, viz., low spin and high spin for a given oxidation state of Ni, based on the branching ratios (β_R) of $L_{3,2}$ edges.[23–25]

In the present study, the energy separation (E_3-E_2) between the L_3 and L_2 edges, which is due to $2p$ spin-orbital splitting, for all the samples is found to be $\sim$17.3 eV in accordance with earlier reports.[15,16,19] The transition energies (E) for both $L_{3,2}$ edges of a Ni film and Ni-Mg films in the metallic state show a small trend towards higher energy from the pure Ni film to a very Mg-rich ($Ni_{0.13}Mg_{0.87}$) film. The spectral profile and branching ratio for the pure Ni film are in good agreement with the previous reports on bulk Ni metal and for Ni films grown on Cu(001) and Co/Cu(001).[16,19] The Ni film was therefore utilized as a reference for Ni-Mg films. The total integrated intensity (A_3+A_2) is smaller and the β_R and A_3/A_2 are larger for Ni-Mg than for Ni (Table I). These results suggest that the addition of Mg produces structural changes and modification of Ni electronic states. Similar results were reported for the Ni film on Cu(001) and Co/Cu(001) due to charge transfer to Ni.[16,19]

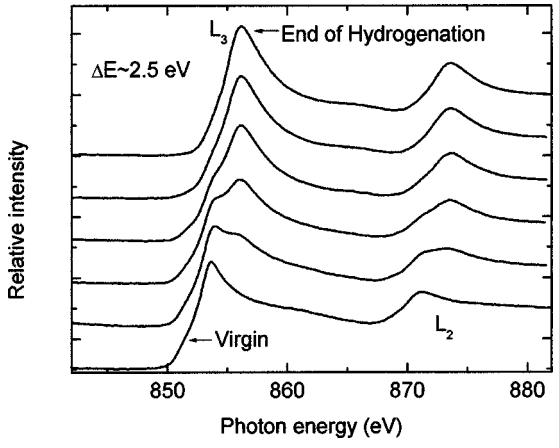

FIG. 2. Transmission mode Ni $L_{3,2}$-edge NEXAS spectra of $Ni_{0.24}Mg_{0.76}$ (262-nm film with 22-nm Pd) film measured in He (denoted as ''virgin'') and in 4% H_2 in He (all other curves) as a function of time. The curve denoted as ''end of hydrogenation'' was recorded after 24 h exposure.

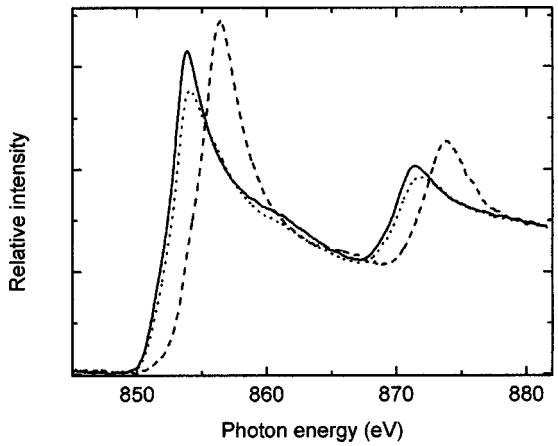

FIG. 3. Transmission mode Ni $L_{3,2}$-edge NEXAS spectra of $Ni_{0.24}Mg_{0.76}$ (262-nm film with 22-nm Pd) film in He (solid line), in 4% H_2 after prolonged hydrogenation (dashed line), and in He after 1 day in air (dotted line).

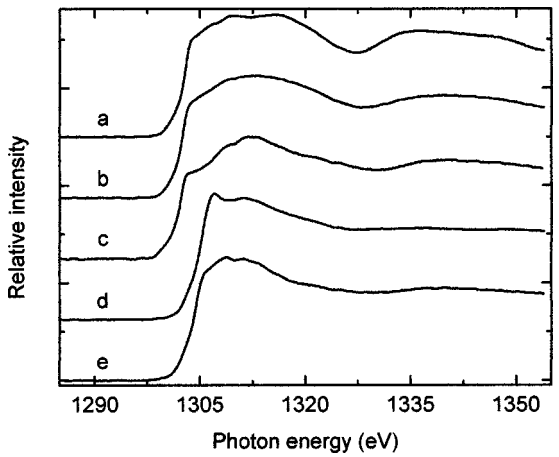

FIG. 4. Transmission mode Mg *K*-edge NEXAFS spectra of thin films in He: (a) Mg (270-nm film with 10-nm Pd), (b) $Ni_{0.13}Mg_{0.87}$ (232-nm film with 11-nm Pd), (c) $Ni_{0.33}Mg_{0.67}$ (154-nm film with 11-nm Pd); in 4% H_2 in He: (d) $Ni_{0.13}Mg_{0.87}$ and (e) $Ni_{0.33}Mg_{0.67}$.

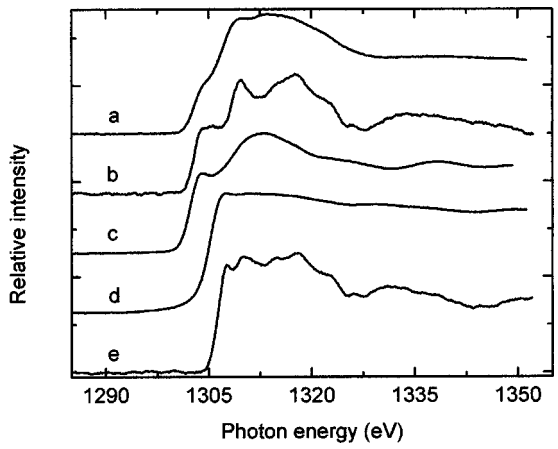

FIG. 5. Mg *K*-edge NEXAFS spectra of (a) 270-nm Mg film with 10-nm Pd (TFY), (b) 45-nm Mg with 10-nm Pd (transmission in He), (c) Mg_2Ni (TFY), (d) MgH_2 (TFY), and (e) 45-nm Mg with 10-nm Pd (transmission in 4% H_2 in He).

Hydrogen uptake by Ni-Mg films caused the transition energies for both $L_{3,2}$ edges to shift significantly towards higher energy by ~2.3 eV for $Ni_{0.33}Mg_{0.67}$ and ~2.6 eV for $Ni_{0.13}Mg_{0.87}$. The total integrated intensity and FWHM also increase. The values for β_R and A_3/A_2 are comparable to those for the Ni film. In general, the effective charge transfer from metal to hydrogen is reported to be less for metal hydrides than for halides, oxides, etc., where the charge transfer is much greater.[29,30] This is supported by the values of β_R and A_3/A_2 for Ni-Mg films in the hydride state, which are comparable to those for the Ni film, indicating that although Ni is in a higher oxidation state, the effective charge transfer in the hydride is less than in the metal. The values of β_R suggest that Ni in hydrided Ni-Mg films is in a high-spin state.[23–25] Hydriding also leads to the creation of nonequivalent Ni sites, which result in larger FWHM's.

B. Mg *K*-edge NEXAFS

Mg *K* near-edge transmission mode spectra of a pure Mg film (270 nm) and two extreme compositions of Ni-Mg films in He and in 4% H_2 are shown in Fig. 4. The Mg *K* edge is shifted to lower energy for Ni-Mg films in the metallic state (1302.2 eV) compared to pure Mg film (1303.0 eV). The intensity of the spectral profile at 1304.5 eV decreases for $Ni_{0.33}Mg_{0.67}$ film when compared to $Ni_{0.13}Mg_{0.87}$ and pure Mg films. Spectra reported for magnesium halides, magnesium oxide, and Mg in minerals and disordered systems show a sharp near-edge peak at ~1310 eV due to the $1s$ to $3p$ transition whose intensity depends on the degeneracy of the $3p$ states. This feature shifts towards higher energy with increasing coordination around Mg.[31–35] In the present study, the transition at 1304.5 eV in pure Mg and Ni-Mg films is assigned to Mg $1s$ to $3p$. The edge shift towards lower energy and reduction in the intensity of the peak with increasing nickel content suggest that the coordination around Mg has decreased, resulting in lowering of the $3p$ degeneracy. The Mg *K*-edge spectra shift toward higher energy by ~2.2 and ~2.9 eV for $Ni_{0.33}Mg_{0.67}$ and $Ni_{0.13}Mg_{0.87}$, respectively, when hydrogen is introduced.

The NEXAFS total fluorescence yield (TFY) spectra for the pure Mg film (270 nm), for Mg_2Ni and MgH_2 powder samples, and a transmission mode spectrum of a thin Mg film (45 nm) in the presence of He and 4% H_2 are shown in Fig. 5. The similarity in the spectral profiles and edge positions for Mg_2Ni and the $Ni_{0.33}Mg_{0.67}$ film are consistent with Mg-Ni bonding in the film. Because transmission measurements are bulk-sensitive, while TFY probes only to about 100 nm in depth, the TFY spectrum for the 270-nm Mg film reflects both Mg and Mg-Pd interface region and the transmission spectrum is dominated by Mg. The transmission spectra of the 45-nm [Fig. 5(b)] and the 270 nm [Fig. 4(a)] Mg films also reflect the presence of different surface and bulk compositions. The near-surface features may be due to Pd-Mg interaction or to formation of an oxide layer prior to Pd deposition.

In addition, the transitions at higher energies due to multiple scattering resonances (see below) were significantly reduced by the presence of hydrogen, which scatters weakly due to its low mass.[36,37] The spectrum of the thick Mg film showed no significant changes on exposure to H_2 for 2 h, consistent with previous observations of very slow diffusion of hydrogen in relatively thick Mg films.[29] The thin Mg film, however, exhibited a 3.5-eV shift following overnight soaking in 4% H_2 at room temperature. This is consistent with optical properties of Mg film with Pd overlayer, which show that an increase in Mg thickness decreases the optical response to hydrogen exposure.[38] The Mg *K*-edge TFY spectrum for bulk MgH_2 also shows a shift of ~2.3 eV towards higher energy compared to the Mg film, consistent with the presence of divalent Mg.

C. Magnesium *K*-edge EXAFS

EXAFS data were analyzed using a background-subtraction method[39–43] with optimization of the low *r* por-

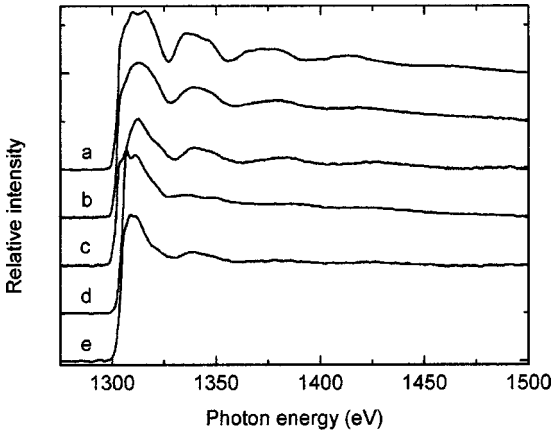

FIG. 6. Mg *K*-edge EXAFS spectra of thin films measured by transmission in He: (a) 270-nm Mg film with 10-nm Pd, (b) $Ni_{0.13}Mg_{0.87}$ (232-nm film with 11-nm Pd), (c) $Ni_{0.33}Mg_{0.67}$ (154-nm film with 11-nm Pd); in 4% H_2 in He: (d) $Ni_{0.13}Mg_{0.87}$, (e) $Ni_{0.33}Mg_{0.67}$.

tion of the EXAFS, followed by Fourier transformation to *r* space. The normalized spectra of the 270-nm Mg film and two Ni-Mg films are shown in Fig. 6. The magnitude of the oscillations decreased with increasing nickel concentration in as-deposited Ni-Mg films due to disruption of the Mg structure. In the hydride state only very weak EXAFS oscillations were observed irrespective of Ni content. Comparison of EXAFS for Ni-Mg films in the hydride and metallic states with bulk MgH_2 and Mg_2Ni (Fig. 7) suggests that more of the magnesium in the $Ni_{0.13}Mg_{0.87}$ film is hydride than in the $Ni_{0.33}Mg_{0.67}$ film, where unreacted Mg_2Ni remains. To get more insight into the structural properties of Ni-Mg thin films, detailed analyses of the experimental EXAFS spectra were conducted by theoretical fits.

Scattering amplitudes and phase shift functions of the Mg-Mg, Mg-Ni, and Mg-O pairs in Mg, Mg_2Ni, and MgO were calculated using the program FEFF (7.02).[40,41] The program FEFFIT (2.5d),[42] which is based on a nonlinear least-squares technique, was used to fit the experimental *r*-space

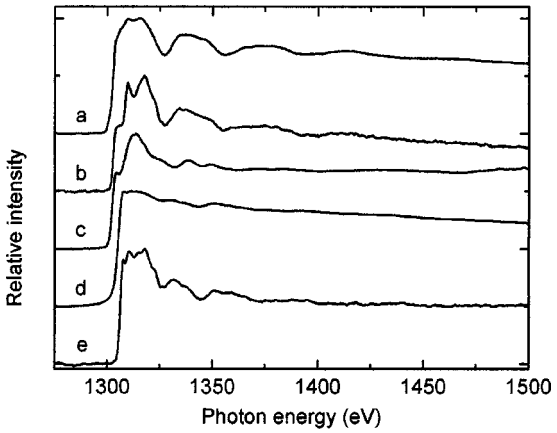

FIG. 7. Mg *K*-edge EXAFS spectra of (a) 270-nm Mg film with 10-nm Pd (transmission in He), (b) 45-nm Mg film with 10-nm Pd (transmission in He), (c) Mg_2Ni (TFY), (d) MgH_2 (TFY), and (e) 45-nm Mg film with 10-nm Pd (transmission in 4% H_2 in He).

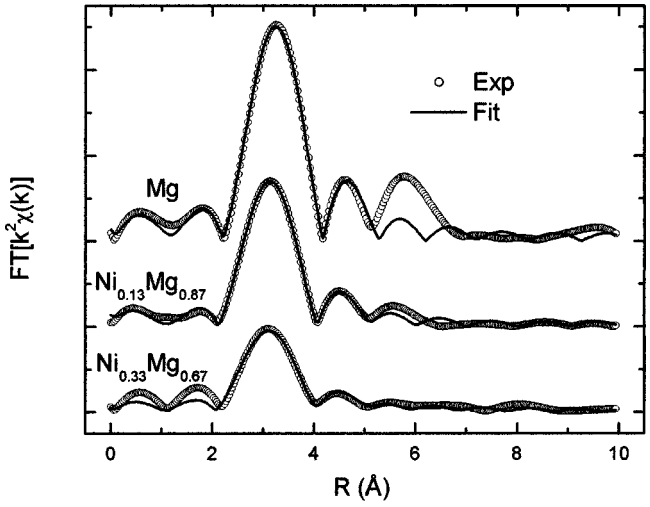

FIG. 8. Phase-corrected and Fourier-transformed Mg *K*-edge EXAFS spectra of 270-nm Mg film with 10-nm Pd, $Ni_{0.13}Mg_{0.87}$ (232-nm film with 11-nm Pd), and $Ni_{0.33}Mg_{0.67}$ (154-nm film with 11-nm Pd) films in the metallic state.

EXAFS data. Phase-corrected Fourier transforms of $\chi(k)$ to *r* space with a k^2 weighting factor and a Hanning window function ($Dk1$ and $Dk2=0.1$) were performed using values of K_{min}, K_{max}, r_{min}, and r_{min} of 1.8 $Å^{-1}$, 5.6$Å^{-1}$, 2.1 Å, and 5.1 Å, respectively. The value of the passive electron reduction factor (S_0^2) (Ref. 43) was deduced from the spectrum of MgO and used for fitting Ni-Mg film spectra.

The Fourier-transformed k^2-weighted Mg *K*-edge EXAFS intensities for Ni-Mg films in their metallic states are presented in Fig. 8 along with theoretical fits. Figure 9 shows the fitting results in *k* space. The resultant structural parameters, coordination number (*N*), bond distance (*R*), and Debye-Waller factor (σ^2) for Mg, $Ni_{0.13}Mg_{0.87}$, and $Ni_{0.33}Mg_{0.67}$ are given in Table II. Attempts were made to fit the data using Mg-Mg (first and second shell), Mg-Ni, and

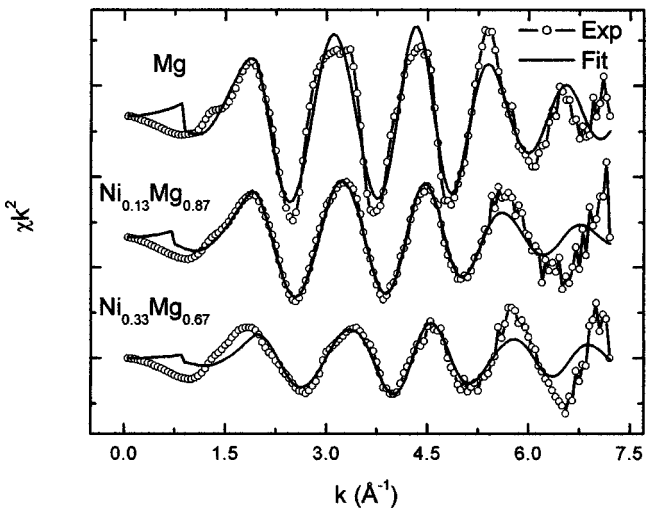

FIG. 9. Fit results in *k* space for Mg *K*-edge EXAFS spectra of 270-nm Mg film with 10-nm Pd, $Ni_{0.13}Mg_{0.87}$ (232-nm film with 11-nm Pd) and $Ni_{0.33}Mg_{0.67}$ (154-nm film with 11-nm Pd); films in the metallic state.

TABLE II. Coordination numbers (N_{Mg}), bond distances ($R_{\mathrm{Mg\text{-}Mg}}$), and Debye-Waller factors ($\sigma^2_{\mathrm{Mg\text{-}Mg}}$) obtained from Mg *K*-edge EXAFS for thin films in metallic state.

	Mg-Mg (first shell)			Mg-Mg (second shell)		
Sample	*N*	*R* (Å)	σ^2 (10^{-2} Å^2)	*N*	*R* (Å)	σ^2 (10^{-2} Å^2)
Mg	12.00(66)	3.203(3)	2.21(19)	4.92(97)	4.568(24)	2.63(19)
$Ni_{0.13}Mg_{0.87}$	8.60(17)	3.098(1)	2.75(7)	2.92(25)	4.465(11)	3.27(7)
$Ni_{0.33}Mg_{0.67}$	3.33(39)	3.038(6)	1.65(35)	1.70(57)	4.472(35)	1.96(35)

Mg-O interactions. No significant contributions from Mg-Ni and Mg-O were found. There is a decrease in amplitude of the Fourier-transformed intensity on the addition of nickel. The nearest-neighbor and next-nearest-neighbor Mg-Mg shells experience a decrease in mean-square relative displacement (MSRD) with increasing nickel concentration. Although the Ni-Mg films are amorphous by XRD, there is microscopic ordering up to the second shell (~4.5 Å), despite decreased coordination numbers and increased disorder with increasing Ni concentration.

The EXAFS oscillations in hydrided films are suppressed for several reasons. The six hydride ions surrounding Mg in MgH_2 are weak scatterers. The number of Mg near neighbors (2 at 3.02 Å) is smaller than in Mg (12 at 3.2 Å), and a second shell (8 at 3.53 Å) causes overlapping oscillations. Finally, the introduction of hydrogen produces a more disordered system. The hydrided 45-nm Mg film shows features similar to those in bulk MgH_2.[6,7] Hydrided Ni-Mg films, however, resemble Mg_2Ni, which suggests that this phase persists even when the free magnesium is converted to MgH_2, and that it dominates the Mg EXAFS spectra. This result is also consistent with the lower optical transparency of films with higher Ni content.

IV. CONCLUSIONS

Cosputtered Ni-Mg films were found to be amorphous. The presence of nickel led to increased disorder and decreased coordination around both Ni and Mg compared to pure metal films. Introducing hydrogen into Ni-Mg films resulted in the formation of Mg-Ni and Mg hydrides, with significant positive x-ray absorption edge shifts. The presence of hydrogen as a near neighbor around Mg produced a drastic reduction in the intensities of multiple scattering (EXAFS) resonances at higher energies. The extent of hydriding depended on the Ni-Mg ratio. A thin pure Mg film was converted to MgH_2. Although the absorption of hydrogen was much slower without nickel, the extent of hydriding was greater. Addition of Ni led to an increase in optical switching speed, a decrease in maximum optical transparency, and a decrease in Mg utilization, probably due to the presence of unreacted Mg_2Ni. Optimization of switching speed and desired transmittance and reflectance ranges will require adjustment of both the Ni-Mg ratio and film thickness.

ACKNOWLEDGMENTS

This work was supported by the Assistant Secretary for Energy Efficiency and Renewable Energy, Office of Building Technology, State and Community Programs, Office of Building Research and Standards of the U.S. Department of Energy under Contract No. DE-AC03-76SF00098. The Advanced Light Source is operated by the Director, Office of Science, Office of Basic Energy Sciences, Division of Materials Science of U.S. Department of Energy under Contract No. DE-AC03-76SF000098 at LBNL. Financial support from the National Science Foundation under Contract Nevada-NSF-EPSCoR is gratefully acknowledged.

*Electronic mail address: tjrichardson@lbl.gov

[1] J. N. Huiberts, R. Griessen, J. H. Rector, R. J. Wijngaarden, J. P. Dekker, D. G. de Groot, and N. J. Koeman, Nature (London) **380**, 231 (1996).
[2] R. Griessen, Europhys. News **32**, 40 (2001).
[3] P. van der Sluis, M. Ouwerkerk, and P. A. Duine, Appl. Phys. Lett. **70**, 3356 (1997).
[4] T. J. Richardson, J. L. Slack, R. D. Armitage, R. Kostecki, B. Farangis, and M. D. Rubin, Appl. Phys. Lett. **78**, 3047 (2001).
[5] T. J. Richardson, J. L. Slack, B. Farangis, and M. D. Rubin, Appl. Phys. Lett. **80**, 1349 (2002).
[6] K. Higuchi, H. Kajioka, K. Toiyama, H. Fujii, S. Orimo, and Y. Kikuchi, J. Alloys Compd. **293-5**, 484 (1999).
[7] K. Yamamoto, K. Higuchi, H. Kajioka, H. Sumida, S. Orimo, and H. Fujii, J. Alloys Compd. **330-2**, 352 (2002).
[8] J. Stöhr, *NEXAFS Spectroscopy* (Springer, New York, 1992).
[9] J. G. Chen, Surf. Sci. Rep. **30**, 1 (1997).
[10] F. M. F. de Groot, Chem. Rev. **101**, 1779 (2001).
[11] D. Wang, A. J. Freeman, and H. Krakauer, Phys. Rev. B **26**, 1340 (1982).
[12] J. Tersoff and L. M. Falicov, Phys. Rev. B **26**, 6186 (1982).
[13] O. Eriksson, A. M. Boring, R. C. Albers, G. W. Fernando, and B. R. Copper, Phys. Rev. B **45**, 2868 (1992).
[14] O. Hjortstam, J. Trygg, J. M. Wills, B. Johansson, and O. Eriksson, Phys. Rev. B **53**, 9204 (1996).
[15] S. S. Dhesi, E. Dudzik, H. A. Dürr, G. van der Lann, and N. B. Brookes, J. Appl. Phys. **87**, 5466 (2000).
[16] P. Srivastava, N. Haack, H. Wende, R. Chauvistré, and K. Baberschke, Phys. Rev. B **56**, R4398 (1997).
[17] J. H. Underwood and E. M. Gullikson, J. Electron Spectrosc. Relat. Phenom. **92**, 265 (1998).
[18] X-ray Data Booklet, Report No. LBNL/PUB490 Rev. 2 (2001) (unpublished).
[19] S. S. Dhesi, H. A. Dürr, G. van der Lann, E. Dudzik, and N. B. Brookes, Phys. Rev. B **60**, 12852 (1999).

[20] S. S. Dhesi, E. Dudzik, H. A. Dürr, N. B. Brookes, and G. van der Laan, Surf. Sci. **454-6**, 930 (2000).
[21] A. I. Nesvizhskii, A. L. Ankudinov, J. J. Rehr, and K. Baberschke, Phys. Rev. B **62**, 15295 (2000).
[22] H. Wang, P. Ge, C. G. Riordan, S. Brooker, C. G. Woomer, T. Collins, C. A. Melendres, O. Graudejus, N. Bartlett, and S. P. Cramer, J. Phys. Chem. B **102**, 8343 (1998).
[23] H. Wang, C. Y. Ralston, D. S. Patil, R. M. Jones, W. Gu, M. Verhagen, M. Adams, P. Ge, C. Riordan, C. A. Marganian, P. Mascharak, J. Kovacs, C. G. Miller, T. J. Collins, S. Brooker, P. D. Croucher, K. Wang, E. I. Stiefel, and S. P. Cramer, J. Am. Chem. Soc. **122**, 10 544 (2000).
[24] H. Wang, D. S. Patil, W. Gu, L. Jacquamet, S. Friedrich, T. Funk, and S. P. Cramer, J. Electron Spectrosc. Relat. Phenom. **114-6**, 855 (2001).
[25] C. Y. Ralston, H. Wang, S. W. Ragsdale, M. Kumar, N. J. Spangler, P. W. Ludden, W. Gu, R. M. Jones, D. S. Patil, and S. P. Cramer, J. Am. Chem. Soc. **122**, 10553 (2000).
[26] B. T. Thole and G. van der Lann, Phys. Rev. B **38**, 3158 (1988).
[27] G. van der Lann and B. T. Thole, Phys. Rev. Lett. **60**, 1977 (1988).
[28] F. M. F. de Groot, Physica B **208-9**, 15 (1995).
[29] M. Gupta and L. Schlapbach, *Hydrogen in Intermetallic Compounds I*, edited by L. Schlapbach (Springer, Berlin, 1988), Chap. 6.
[30] R. Yu and P. K. Lam, Phys. Rev. B **37**, 8730 (1988).
[31] S. Naoé, T. Murata, and T. Matsukawa, Physica B **158**, 615 (1989).
[32] T. Yoshida, T. Tanaka, H. Yoshida, T. Funabiki, and S. Yoshida, J. Phys. Chem. **100**, 2302 (1996).
[33] H. Aritani, T. Tanaka, T. Funabiki, S. Yoshida, M. Kudo, and S. Hasegawa, J. Phys. Chem. **100**, 5440 (1996).
[34] H. Aritani, H. Yamada, T. Nishio, T. Shiono, S. Imamura, M. Kudo, S. Hasegawa, T. Tanaka, and S. Yoshida, J. Phys. Chem. **104**, 10 133 (2000).
[35] P. Ildefonse, G. Calas, A. M. Flank, and P. Lagarde, Nucl. Instrum. Methods Phys. Res. B **97**, 172 (1995).
[36] R. R. G. Agostino, G. Liberti, V. Formoso, E. Colavita, A. Züttel, C. Nützenadel, L. Schlapbach, A. Santaniello, and C. Gauthier, Phys. Rev. B **61**, 13 647 (2000).
[37] B. Lengeler, Phys. Rev. Lett. **53**, 74 (1984).
[38] T. J. Richardson, B. Farangis, and J. L. Slack (unpublished).
[39] M. Newville, P. Livins, Y. Yacoby, J. J. Rehr, and E. A. Stern, Phys. Rev. B **47**, 14 126 (1993).
[40] A. L. Ankudinov and J. J. Rehr, Phys. Rev. B **56**, R1712 (1997).
[41] A. L. Ankudinov, Ph.D. thesis, University of Washington, 1996.
[42] E. A. Stern, M. Newville, B. D. Ravel, Y. Yacoby, and D. Haskel, Physica B **208-9**, 117 (1995).
[43] E. A. Stern and S. M. Heald, in *Handbook on Synchrotron Radiation*, edited by E. E. Koch (North-Holland, New York, 1983), Vol. 1.